3D imaging of undissected optically cleared *Anopheles stephensi* mosquitoes infected with *Plasmodium* parasites

Mariana De Niz[1*], Jessica Kehrer[2], Nicolas M.B. Brancucci[3#], Federica Moalli[4Δ], Emmanuel G. Reynaud[5], Jens V. Stein[4§], Friedrich Frischknecht[2]

[1] Institute of Cell Biology, Heussler Research Group, University of Bern, Bern, Switzerland

[2] Center for Infectious Diseases, Integrative Parasitology, University of Heidelberg Medical School, Heidelberg, Germany

[3] Wellcome Centre for Integrative Parasitology, Institute of Infection, Immunity & Inflammation, University of Glasgow, Glasgow, UK

[4]Theodor Kocher Institute, University of Bern, Bern, Switzerland

[5] School of Biomolecular and Biomedical Science, University College Dublin, Ireland

[*] Current address: Instituto de Medicina Molecular João Lobo Antunes, Faculty of Medicine, University of Lisbon, Portugal

[#] Current address: Swiss Tropical and Public Health Institute, University of Basel, Basel, Switzerland

[Δ] Current address: San Raffaele Scientific Institute, Milan, Italy

[§] Current address: Department for Oncology, Microbiology and Immunology, University of Fribourg, Switzerland

Corresponding author: Mariana De Niz mariana.deniz@medicina.ulisboa.pt

Abstract

Malaria is a life-threatening disease, caused by Apicomplexan parasites of the *Plasmodium* genus. The *Anopheles* mosquito is necessary for the sexual replication of these parasites and for their transmission to vertebrate hosts, including humans. Imaging of the parasite within its insect vector has been attempted using multiple microscopy methods, yet most have been hampered by the presence of the mosquito's opaque cuticle, which scatters light. So far, imaging of the *Plasmodium* mosquito stages has depended on either sectioning or surgical dissection of important anatomical sites, such as the midgut and the salivary glands. Optical projection tomography (OPT) and light sheet fluorescence microscopy (LSFM) enable imaging fields of view in the centimeter scale whilst providing micrometer resolution. In this paper, we present reconstructions of the whole body of *Plasmodium*-infected, optically cleared *Anopheles stephensi* mosquitoes and midguts. The 3D-reconstructions from OPT imaging show detailed features of the mosquito anatomy relevant for transmission, and enable overall localization of the parasite within the vector throughout the entire mosquito life cycle. Additionally, LSFM imaging of mosquito midguts shows detailed distribution of oocysts in the midgut of intact mosquitoes.

Introduction

Arthropod-borne diseases constitute an enormous public health burden world-wide. Some of the most medically relevant diseases in tropical areas caused by mosquitoes include malaria, dengue, yellow fever, chikungunya fever, Zika fever, encephalitis, and filariasis (Beaty and Marquardt, 1996; Eldridge and Edman, 2000; Kettle, 1995; Lehane, 1991). The blood-sucking behavior of female mosquitoes is necessary for egg development and constitutes the link to vertebrate hosts, as pathogens are transmitted during mosquito blood meals. There are approximately 3,500 species of mosquitoes grouped into two main sub-families and 41 genera (CDC, 2014). The two subfamilies are the *Anophelinae* and the *Culicinae*, which not only display important anatomical and physiological differences, but vary in their clinical significance as disease vectors of the pathogens they transmit. Recent outbreaks of Zika and dengue fever, as well as the constant pressure of malaria on many regions

of the developing world continue to demand a better understanding of host-pathogen interactions in the vector. Advances in this field are likely to inform researchers across various disciplines about improved ways of blocking pathogen transmission. In this paper we focus on 3D imaging of intact (in contrast to dissected), optically cleared *Anopheles* mosquitoes as vectors for the *Plasmodium* parasite, the causing agent of malaria. We envisage that the technique is equally useful to *Aedes* and *Culex* mosquitoes, both of which are important vectors of a wide range of pathogens.

Malaria currently causes over 400,000 deaths per year in humans (WHO, 2016). Although hundreds of vertebrate-infecting *Plasmodium* species exist, only five species are infectious to humans. During their life cycle *Plasmodium* parasites adopt various forms, both invasive and replicative, within the vertebrate host and the mosquito vector (reviewed by (Aly et al., 2009; Silvie et al., 2008)). Imaging of the malaria parasite within the living mosquito has remained elusive and limited to observe the passive floating of sporozoites in the hemolymph and proboscis (Frischknecht et al., 2014, 2006). The development of sporozoites *in vivo* in the midgut and their entry into mosquito salivary glands remains to be visualized. As these organs are surrounded by an optically opaque cuticle most of the imaging achieved so far has relied on dissection of these organs and imaging *in situ*.

The possibility to visualize biological tissue in 3D has proven to be invaluable for understanding complex processes in various tissue forms – including that of insects. For centuries, imaging at depth required the physical sectioning of tissue due to photon scattering. The imaging limit of conventional microscopy in terms of penetration depth, is set by a physical parameter of a photons known as the mean free path (MFP) (reviewed by Ntziachristos, 2010). The MFP translates as the number of scattering or collision events that a photon undergoes, which modify the photon's properties and result in image blurring. For widefield epifluorescence microscopy (**Figure 1A**), the thickness of tissue sections is 10-50 μm, which ensures diffraction-limited resolution. Confocal (**Figure 1B**) and multi-photon microscopy allow greater penetration depths of up to 500 μm. Nevertheless, a highly resolved 3D digital reconstruction would require acquisition of hundreds of individual thin sections and long imaging periods during which the sample must be under high energy illumination. This renders confocal and multiphoton techniques impractical for imaging intact, large specimens.

Novel 3D imaging techniques such as optical projection tomography (OPT) and light sheet fluorescence microscopy (LSFM) also known as selective plane illumination microscopy (SPIM) or Ultramicroscopy, allow visualization of large objects without the need of physical sectioning. A pre-requisite for these imaging techniques applied to opaque samples is optical clearance, as in transparent media light propagates deeper into tissues, overcoming photon scattering to a major extent (reviewed by (Ntziachristos, 2010). In order to generate a transparent sample, tissues can be chemically cleared with various solvents (reviewed by (De Niz et al., 2019)).

After rendering the specimen transparent, OPT imaging is achieved via tissue trans- and epi-illumination over multiple projections (Sharpe et al., 2002) as the specimen is rotated through 360 degrees in angular steps around a single axis **(Figure 1C)**. Virtual sections are reconstructed from the acquired images using a back-projection algorithm (Kak and Slaney 1988). Altogether, OPT achieves penetration depths of up to 15 millimeters (Sharpe et al., 2002), and high resolution 3D image reconstructions of the sample's complete volume can be obtained.

Conversely, LSFM uses a thin plane of light (or light sheet), that is shaped by a cylindrical lens or a laser scanner to exclusively illuminate the focal plane of the sample at any one time (**Figure 1D**) (Huisken et al., 2004). While in conventional microscopes illumination and detection follows the same path, the detection pathway in LSFM is rotated by 90 degrees. LSFM displays high imaging speed, reduced toxicity, and reduced photobleaching (reviewed by Pampaloni et al., 2007). 3D image formation is based on raw images being assembled after translation or rotation of the entire sample either in a step-wise manner or Multiview mode. Multiple LSFM setups have been developed, including OPTiSPIM (Mayer et al., 2014), a hybrid setup which combines the high resolution of SPIM with the possibility to image fluorescent and non-fluorescent contrasts of OPT. The difference between OPT and LSFM in terms of mesoscopic imaging, is that OPT images are isotropic (without distortion in any 3D axis), but the focal depth is deliberately large, with low numerical aperture (NA) objectives (low resolution). Conversely, LSFM images are anisotropic (with higher resolution in the xy axes than in *z*), but usually work with higher NA objectives, and therefore achieve a high resolution, up to single cell level. OPT can also be designed for single cell resolution, but at the expense of sample size imaging capacity.

Open source, custom built-versions and free software for LSFM (OpenSPIM) (Gualda et al., 2013; Pitrone et al., 2013) and OPT (OptiJ) (Vallejo Ramirez et al., 2019) have been generated, making these imaging platforms easily accessible across labs and disciplines.

OPT and/or LSFM have been used to image various specimens (reviewed in (De Niz et al., 2019)) including a detailed reconstruction of the anatomy of the flight musculature of a *Drosophila* fly, its nervous and digestive systems, and ß-galactoside activity throughout the fly's whole body (Jährling et al., 2010; McGurk et al., 2007). Using OPT or LSFM, fluorescence reporters and antibody labeling can be used to reveal specific structures or protein localizations.

Recent work for the first time showed *P. berghei* development at fixed points in optically cleared mosquitoes using CUBIC (Mori et al., 2019). In our work, 3D reconstructions of optically cleared *Anopheles stephensi* mosquitoes infected with mCherry- or GFP-expressing *Plasmodium berghei* parasites were performed using OPT and LSFM. We also present a comparative evaluation of different clearance protocols, which possess different advantages depending on the scientific question of interest, and are differently relevant upon the use of autofluorescence detection alone, or the detection of fluorescent dyes, antibodies, and/or reporters.

The reconstructions we present here are based on mosquitoes rendered transparent using Murray's clear. They provided detailed insight into the anatomy of the mosquito head, thorax and abdomen. We envisage that the presented techniques will be of great use in the fields of pathogen and vector biology.

Materials and Methods

Ethics statement

Mouse infections were carried out under the approval of the Animal Research Ethics Committee of the Canton Bern, Switzerland (Permit Number: 91/11 and 81/11); the University of Bern Animal Care and Use Committee, Switzerland; and the German Tierschutzgesetz (Animal Rights Laws). For all mosquito feeds, female mice 5–8 weeks of age, weighing 20-30 g at the time of infection were used. Mice were purchased from Harlan or Charles River laboratories. Blood feeding to

mosquitoes was performed under ketavet/dorbene anaesthesia, and all efforts were made to minimize animal suffering.

Parasites lines and their maintenance in mosquitoes

P. berghei-ANKA lines were used in this study to infect mice used for mosquito feeds. *P. berghei*-mCherry$_{Hsp70}$ (Burda et al., 2015), *P. berghei*-GFP$_{Hsp70}$ and PbmCherry$_{Hsp70}$FLuc$_{ef1\alpha}$ (Prado et al., 2015) express fluorescent mCherry that localizes to the cytosol of the parasite, and is expressed constitutively throughout the parasites' life cycle.

Balb/c mice were treated with phenylhydrazine two days prior to intra-peritoneal (i.p.) infection with *P. berghei*-mCherry$_{Hsp70}$ or PbmCherry$_{Hsp70}$FLuc$_{ef1\alpha}$. After 3 days of infection, gametocyte exflagellation was assessed. Upon confirming exflagellation, the infected mice were used to feed 100–150 *Anopheles stephensi* female mosquitoes. Mice were anaesthetized with a combination of Ketasol/Dorbene anaesthesia, and euthanized with CO_2 after completion of the feed. Afterwards, mosquitoes were fed until use, with 8 % fructose containing 0.2 % PABA.

Mosquito embedding

Adult female *Anopheles stephensi* mosquitoes were killed at various times following feeds on mice infected with *P. berghei,* and fixed overnight at 4°C in a 1:1 mixture of 4% paraformaldehyde in 1x PBS and 100% ethanol. Mosquitoes were then washed 3 times in 1xPBS for 5 minutes each time. Washed mosquitoes were embedded in 1.3% ultrapure low-melting agarose (Invitrogen) in deionized water. Gels containing the mosquitoes were transferred for at least 2h to 4°C. Using a single-edge blade, the gel was then trimmed into a block containing a single mosquito in the centre.

BABB (Murray's clear)-based mosquito dehydration and clearance

Agarose blocks containing the mosquitoes at all times post blood-feed (including 2 h, 20 h, and day 1 through day 16), were dehydrated in a graded ethanol series (50, 70, 90, 96, and 100%) for 1 h each. Mosquitoes were then transferred to another flask containing 100% ethanol, and dehydrated overnight. Finally, mosquitoes were incubated in a clearing solution consisting of two parts benzyl

benzoate and one part benzyl alcohol (BABB, also known as Murray's clear) (Dodt et al., 2007; Genina et al., 2010; Gerger et al., 2005) for at least 10 days, until they became transparent.

3DISCO-based mosquito dehydration and clearance

Previous work showed that tetrahydrofluoran (THF) in combination with dibenzyl ether (DBE), fully clears multiple mouse tissues including the lymph nodes, spinal cord, lungs, spleen and brain, while successfully preserving fluorescent signals (Becker et al., 2012; Ertürk et al., 2012). Two clearing protocols were adapted for use in mosquitoes, namely a relatively short protocol consisting of dehydration in a graded THF series (50, 70, 80 and 100%) for 30 minutes each, followed by 2 further 30 minute incubations in 100% THF. This was followed by a 20-minute incubation in dichloromethane (DCM), and a 15-minute incubation in DBE. The long protocol consisted on dehydration in the graded THF series for 12 h each, followed by 2x 12 h incubations in 100% THF. This was followed by a 5-day clearance in DBE, without the intermediate DCM step.

SeeDB-based mosquito dehydration and clearance

In 2013, Ke and colleagues (Ke et al., 2013) first published a water-based optical clearing agent called SeeDB, which had the advantage of preserving fluorescence, including that of lipophilic tracers, while also preserving sample volume and cellular morphology. In order to prepare fructose solutions, D(-)-fructose was dissolved in distilled H_2O at 65°C, and upon cooling to 25°C, α-thioglycerol was added to give a final concentration of 0.5%. Mosquitoes were initially fixed in 4% PFA, and embedded into 1% ultrapure agarose in dH_2O. Fixed mosquitoes were then serially incubated in 20%, 40% and 60% fructose, each for 4 h, followed by a 12 h incubation in 80% fructose, a 12 h incubation in 100% fructose, and a 12 h incubation in SeeDB at either 37°C or 50°C.

Microscopy – Optical projection tomography (OPT)

OPT scanning was performed according to the manufacturer's instructions (Bioptonics). Filter sets were exciter 425/40, emitter LP475 for autofluorescent signal, exciter 480/20, emitter LP515 for green fluorescent signal; and exciter 545/30, emitter 617/75 for red fluorescent signal. Raw data were

converted into 3D voxel datasets using NRecon software from Bioptonics. Reconstructed virtual *xyz* data sets were exported as .tif files and analyzed with IMARIS (Bitplane) for visualization and/or isosurface reconstruction of parasite distribution in the mosquitoes. IMARIS reconstructions were carefully adjusted to fit original NRecon reconstructions.

Light Sheet Fluorescence Microscopy (LSFM)

Light sheet fluorescence microscopy scanning was performed using a commercially available Ultramicroscope system (LaVision BioTec). Light was produced by a 200-mW laser that illuminates the sample from both sides by two co-localized thin sheets of light to compensate for absorption gradients within the tissue. A 10x objective with a NA of 0.3 was used.

Microscopy - Confocal imaging

Confocal imaging of dissected midguts and salivary glands for validation of the observations performed by OPT and LSFM was performed using a Leica SP8-STED microscope. Midguts and salivary glands were imaged using a 20x air objective, using a white light laser at a wavelength of 550nm, and a 63x oil immersion objective using a white laser at wavelengths 405 and 488 nm. The LASX software was used for image acquisition.

Sample mounting for OPT and LSFM

Microscope setups for conventional widefield and confocal systems are remarkably different to those of OPT and LSFM (**Figure 1**). For conventional fluorescence microscopy samples are usually placed on glass bottom dishes or microscope slides in which they are overlayed with a coverslip. Preparation for OPT and LSFM requires placing the sample in a medium- or liquid-filled chamber that enables rotation or motion during image acquisition (**Figure 2A**). In order to take full advantage of the 3D imaging technique all the specimens need to be mounted into a special metal sample holder that is inserted into the chamber from a magnet above (**Figure 2B**). The specimen may be embedded in a gel such as low melting agarose dissolved in the medium or buffer of choice (**Figure 2C**). The medium keeps the sample in place without influencing the penetration of light and imaging quality.

Results and Discussion

Optical clearance of infected and uninfected *Anopheles stephensi* mosquitoes

One of the major hurdles for whole-body mosquito imaging is light scattering due to presence of the cuticle. The cuticle forms the major part of the integument of mosquitoes. Its functions include on one hand reducing the risk of water evaporation from the insect's body, and protecting internal organs from damage or bacterial infections. On the other hand, it also enables maintaining the insect's shape while allowing rapid motion. Although across most of the mosquito body the cuticle is rigid, between the different body segments, and at the joints of limbs and other appendages, it is flexible to allow movement.

In terms of composition, the integument is made of a single layer of ectodermal epithelium, that is attached to a non-cellular internal membrane called the basement membrane. The layer of epithelium on the basement membrane produces the cuticle, which begins as a tough, flexible layer of chitin. Such thin and elastic chitin is used as a major structural part where the integument requires great flexibility, such as in bodily parts that must stretch to contain accumulated liquids, or that form joints between rigid parts of the exoskeleton. In other parts of the cuticle, such as the mosquito thorax, the function of the integument demands more rigid materials. To achieve such rigidity the outer chitin layer of the cuticle is reinforced with harder, more brittle materials such as sclerotinised proteins or calcite.

Optical clearing enables an increase of light depth penetration. Techniques for optical clearing generally reduce light scattering by replacing cellular water with solutions that have a refractive index similar to that of the cell membrane. Lipids in cell membranes are dominant scattering agents in biological tissues, and optical clearing methods can obtain approximately uniform refractive index profiles by removing them. Reduced light scattering ultimately leads to higher spatial resolution and greater contrast. Various clearance techniques have been developed, and have proven to be advantageous for imaging different tissues of interest. These techniques include the use of organic solvents (Abe et al., 2016; Becker et al., 2012; Dodt et al., 2007; Ertürk et al., 2012), water ((Hama et al., 2015, 2011; Ke et al., 2013), and electrophoresis-based protocols (Chung et al., 2013; Poguzhelskaya et al., 2014). In this paper, four techniques were used for mosquito clearance, and were

compared in terms of a) time to achieve tissue transparency, b) preservation of fluorescence signal in mosquitoes infected with mCherry-expressing *Plasmodium berghei* parasites and c) resulting mosquito tissue morphology following treatment. These methods are BABB (Murray's clear), Sca*l*eS, SeeDB, and 3DISCO. Results are summarized in table 1 below. Among the clearance protocols tested, only the two solvent-based protocols (BABB and 3DISCO) achieved transparency of the mosquito cuticle within 3 or 30 days respectively. 3DISCO is an organic solvent-based method using tetrahydrofluorane and DBE, which has been reported to successfully preserve fluorescence in brain mouse tissues, while enabling adequate levels of tissue clearance (Ertürk et al., 2012). In mosquitoes, the cuticle was only successfully cleared after up to 30 days of incubation. However, fluorescence signal from the midguts, as assessed using an epifluorescence microscope, was gradually lost. Although mosquito tissue morphology was well preserved, the long incubation time needed to achieve clearance, and the loss of fluorescence led us to exclude this method for further work. Next, we tested Sca*l*eS, a sorbitol-based clearance protocol renowned for its successful preservation of tissue morphology and fluorescence signal (Hama et al., 2015). Although we noticed that in treated mosquitoes morphology and fluorescence were indeed optimally preserved, clearance was only partial after 30 days of sample incubation, showing that although the method could be successfully applied for use in brains and samples of similar composition, it was suboptimal for clearance of the mosquito cuticle. We also tested SeeDB, a protocol that combines use of the water-soluble clearing agents fructose and urea. SeeDB has been reported to achieve fast clearing results of brain tissue with optimal preservation of tissue integrity and fluorescence signal (Ke et al., 2013). As for Sca*l*eS, although mosquito tissue preservation and fluorescence signal were indeed optimally preserved with SeeDB, we found that clearance of the cuticle was only partial after a month of incubation. Finally, we tested the organic-solvent-based Murray's clear method (BABB), which uses benzyl alcohol and benzyl benzoate as organic solvents. This method achieved the fastest clearance of the mosquito cuticle but led to slight shrinkage of the tissue due to dehydration. Unexpectedly, it enabled preservation of mCherry fluorescence signal during extended time periods. Notably, when mosquitoes were infected with GFP-expressing *P. berghei* parasites, fluorescence was significantly lost, suggesting that different fluorescent proteins would react differently to this clearance method, as previous work has also suggested (Abe et al., 2016).

Considering the overall performance in tissue clearance, BABB was the method of choice for all subsequent experiments reported in this work.

Table 1. Comparison of clearing methods for mosquito cuticle

Method	Principle	Time to achieve tissue transparency	Preservation of fluorescence signal	Preservation of tissue morphology
3DISCO	Organic solvent	20-30 days (++)	+/-	Unaltered
BABB (Murray's clear)	Organic solvent	5-10 days (+++)	++	Slight dehydration
ScaleS	Water-based	Partial clearance at 30 days (+/-)	+++	Unaltered
SeeDB	Water-based	Partial clearance at 30 days (+/-)	+++	Unaltered

OPT enables visualization of the entire anatomy of intact adult mosquitoes

Cleared adult *Anopheles stephensi* mosquitoes were three-dimensionally reconstructed from OPT projections (**Figure 3A-B; Movie 1**), to represent various features of the head, the thorax, and the lower body including the midgut *in situ*. Following clearance, absorption, reflection and auto-fluorescence of the cuticle were reduced to an extent that internal organs of the mosquito could be visualized (**Figure 3**). The vectorial capacity of different mosquito families in general, and *Anopheles* species in particular, is governed by features intrinsic to the mosquito's biology, including longevity, blood-feeding preferences, and immune responses to pathogens (Mitchell et al., 2015). As proof of concept, in this work we imaged unlabelled mosquitoes, and visualized their anatomical features solely by using tissue autofluorescence. Nevertheless, we envisage that many of the mosquito's physiological and anatomical features could be specifically labelled with antibodies or fluorescent tagging, and visualized in wild type and mutant mosquitoes exposed to a plethora of vector-borne pathogens.

The mosquito head is specialized for sensory information, and feeding. The mosquito has compound eyes made up of multiple lenses called ommatidia, which could be faithfully reconstructed by OPT (**Figure 3C, top panels**). Although we did not attempt to employ LSFM for higher resolution imaging of these compound eyes, it is known that each individual ommatidium has a cornea, a lens, and

photoreceptor cells all of which enable vision. Moreover, each ommatidium is set at different angles, allowing sensitive detection of movement in the mosquito's surroundings. Potential prospective work using LSFM may likely allow visualization of these detailed features at greater resolution than that achieved by OPT.

Olfaction is an additional primary sensory modality of mosquitoes. Vectors such as *Anopheles* mosquitoes, are guided to human hosts by olfactory cues released from the human body (Reviewed by (Takken and Knols, 1999)). Macro-scale imaging tools have led to the identification of structures in the mosquito anatomy involved in processing of thermal and olfactory sensory inputs. These tools led to the discovery that, aside of the antennae and the maxillary palps, the proboscis is fundamentally involved in thermo-sensing and therefore essential for host target recognition (Maekawa et al., 2011). OPT enabled imaging of setae (hair-like structures) on the antennae, the mandibles and maxillae lining the alimentary canal, and the maxillary palps (**Figure 3C, top panels**). Changes in insect sensory responses and behavior are likely to increase the chances of parasite transmission, and are thought to arise either from either changes in the expression of salivary gland components (Choumet et al., 2007; Ribeiro et al., 1984; Rossignol et al., 1984), or from the modulation of the mosquito nervous system by, for instance the *Plasmodium* parasite (Lefevre et al., 2007). While mosquito imaging has largely focused on the sites of parasite replication and residence i.e., the midgut and salivary glands, respectively, imaging of specific molecules and gene expression levels in other tissues that potentially influences behaviour has not yet been performed but could be achievable with OPT or LSFM.

Following attraction to the host and target-finding, the mosquito must ensure fast and efficient blood feeding. Mosquitoes possess a chemosensory apparatus within the proboscis, called the stylet that harbors olfactory receptors able to respond to volatile compounds in the host blood (reviewed by (Krenn and Aspöck, 2012), (Won Jung et al., 2015)). Other structures equally relevant in the feeding process are the cibarial and pharyngeal dilator pumps, which control movement of the blood meal into the gut. A valve-like organ is located between both of these pumps and prevents backflow in the conduit connecting both structures. Relevant to blood feeding behaviours, the recent implementation of synchrotron X-ray microscopic computed tomography in malaria research, allowed for a detailed description of the feeding pump system located inside the head of *Anopheles* and *Aedes* mosquitoes (Ha

et al., 2015). The study concluded that morphological and functional features of the pump system strongly influence the feeding behaviour of female mosquitoes, therefore influencing the transmission success of various pathogens to humans. While techniques such as scanning electron microscopy and synchrotron X-ray tomography have provided important findings on the anatomy of the mosquito head, both require complex equipment and sample preparation. OPT requires not only relatively simple sample preparation but in contrast to the aforementioned techniques, is also compatible with the use of fluorescent probes and dyes. We envisage that imaging of intact optically cleared mosquitoes using the absorption mode of OPT (ie using ß-galactosidase-dependent blue staining) will enable tracking pathogen-induced changes in gene expression (Sharpe et al., 2002), and changes in expression of specific components in the mosquito's sensory systems, which may be responsible for changes in vector behavior.

The *Anopheles* mosquito thorax is specialized for locomotion, and is divided into three segments, namely the prothorax, the mesothorax, and the metathorax, all of which were easily distinguished by OPT (**Figure 3B**) (The surface rendered image has been previously shown in (De Niz et al., 2019)). Each thoracic segment supports a pair of legs (3 pairs in total), while the mesothorax additionally bears a pair of wings (**Figure 3C, bottom panels)**. Moreover, the thorax harbours the dorsal blood vessel, the tracheal and dorsal tubes (or heart), the foregut, and various nerve ducts (**Figure 3A-3B**).

Finally, the abdomen (**Figure 3A-3B**) is specialized for food digestion, reproduction, and egg development. The *Anopheles* mosquito abdomen is long and can be divided into up to 10 segments, clearly visible by OPT (**Figure 3B, right panel**). Unlike the thorax, segments I to VIII are able to expand significantly upon ingestion of a blood meal. Segment VIII bears the terminal anus of male and female mosquitoes. In females, segments IX and X bear the gonopore, and a post-genital plate, while in males, segments IX and X harbour a pair of clawed claspers and an aedigus. The vectorial capacity of *Anopheles* mosquitoes, or their capacity to transmit the parasite, is largely determined by the mosquito's reproductive success (Macdonald, 1956; Smith et al., 2012). Multiple studies have linked the mosquito's seminal secretions (particularly the steroid hormone 20-hydroxyecdysone (20E)) with multiple entomological parameters in females, including mosquito densities via the protein Mating-

Induced Stimulator of Oogenesis (MISO)- a stimulator of oogenesis (Baldini et al., 2013). These are lipid transporters that favour *Plasmodium* development by altering the mosquito's immune system (Rono et al., 2010) and longevity due to reduced mating-associated fitness costs. A recent study linked MISO and 20E levels to phylogenetic diversity and transmission success of multiple *Anopheles* species, showing that species producing high titres of 20E are the most successful malaria transmitters (Mitchell et al., 2015). Tracking of hormones such as 20E in *Anopheles* and other mosquito families, including *Aedes* and *Culex* by OPT and LSFM in a high-throughput context may become an important application for researchers studying the transmission of mosquito-borne pathogens.

Internally, the abdomen harbours the ovaries and oviduct in females, the hind-gut, the Malpighian tubules, and the midgut (or stomach). The latter is of pivotal importance for replication of pathogens including *Plasmodium* and various viruses including West Nile, Chikungunya, and dengue. Labeling the midgut as well as other anatomical structures with specific antibodies, or cell type-specific fluorescent reporters in both mosquitoes and pathogens would be a valuable tool for studying host-pathogen interactions at a whole-body level.

OPT enables imaging *Plasmodium* development within the undissected mosquito midgut and the salivary glands.

We used mCherry- or GFP-tagged *P. berghei* to observe parasite distribution within entire mosquitoes at various times post blood-feed. We performed parallel imaging of the isolated mosquito midguts by LSFM (**Figure 4**) and an OPT time experiment using intact mosquitoes. During a blood meal on their infected vertebrate hosts, mosquitoes ingest *Plasmodium* parasites including the transmission-competent sexual stages, called gametocytes. These initiate the sporogonic cycle after female and male gametocytes give rise to sexual gametes, which fertilize in the midgut lumen within one hour following ingestion. Various imaging methods have shown that the resulting zygotes develop into motile ookinetes, which invade and traverse the midgut epithelium within 24 h following ingestion. Ookinetes reach the basal side of the mosquito midgut, where they transform into oocysts within the first 72 h post-feed. These then undergo multiple rounds of mitosis as they mature (within a time frame of 12 to 16 days). At maturity, each oocyst releases thousands of haploid sporozoites that travel through

the haemolymph and eventually invade the mosquito salivary glands. Upon a blood feed on a vertebrate, and the concomitant injection of the saliva into the vertebrate's skin, infectious sporozoites are transmitted into the new host (Reviewed by (Whitten et al., 2006)). OPT allowed visualization of diverse parasite localizations within infected mosquitoes. The initial and final days are shown.

At day 1 immediately after a feed on an infected mouse, no fluorescent signal from parasites was detected, yet the mosquito anatomy can be visualized at high level of detail. At day 16 post-infection, we detected strong mCherry signals in the salivary glands, the mesothorax, the base of the wings, and the midgut (**Figure 4A**). **Figure 4B** shows LSFM performed on midguts and shows *P. berghei* oocysts across a full rotation of the sample. **Figure 4C** shows the level of detail obtained by OPT across different sections of the cleared mosquito. While our work provides a proof of principle, higher resolution OPT and LSFM could become valuable methods to study yet unanswered questions, including the hypothesis that once in the vicinity of the salivary glands, the location and invasion of the glands depends on short-range chemotactic and/or receptor-ligand interactions (Akaki; Oelerich 1967; Devreotes and Zigmond 1988; Taylor 1999). *In situ* imaging of parasite motion in different genetic contexts (genetically engineered mosquitoes and/or *P. berghei*) may be used to unravel this and other important aspects of host-parasite interactions.

Imaging of the parasites requires adequate clearance of the mosquito tissue and cuticle, while enabling preservation of fluorescence of the parasite (as described previously). We found that eggs in the abdominal cavity of adult females are heavily auto-fluorescent and thereby can obscure the midgut. While mCherry fluorescence was successfully preserved, GFP fluorescence dropped substantially during clearance using BABB. This suggests that for visualization of host-pathogen interactions, or imaging of multiple mosquito or *Plasmodium* proteins by multi-colour labeling or tagging using different fluorescent proteins, BABB might be a rather aggressive clearing method, potentially hampering activity of some fluorophores. Recently, CUBIC (Abe et al., 2016; Susaki et al., 2016) was shown to better preserve fluorescence while also achieving successful clearance of tissues. Therefore, this method may become a suitable option for multi-colour imaging of cleared mosquitoes containing fluorescently tagged parasites as recently shown (Mori et al., 2019). Potential technical improvements include OPTiSPIM, a method combining the advantages of transmission OPT with the high resolution

of SPIM imaging (Mayer, J. et al, 2014). We envisage that any of the individual or combined 3D imaging approaches will allow for large throughput analyses and visualization of detailed host-pathogen interactions in the context of a number of tropical diseases including dengue and Zika virus infections, lymphatic filariasis, yellow fever, and malaria.

Conclusion

At present live cell imaging of parasite development the mosquito is highly limited due to the presence of the mosquitoes' opaque cuticle which acts as a major light scatterer. Here, we have shown that adult *Anopheles* mosquitoes can be cleared efficiently, and that this allows for transmission of white and fluorescent light to detect detailed mosquito anatomical features in 3D using OPT and LSFM. This dataset might be used as an anatomical framework onto which pathogen-induced gene expression patterns could be mapped. Further, we are convinced that our results constitute the basis for following the localization and development of different mutant pathogens within their mosquito host. This opens up the possibility of imaging infection events in mosquitoes, which may allow studying phenotypes of mutant pathogens incapable of completing their life cycle within the insect vector, as well as deciphering the role of mosquito genes in pathogen survival and behaviour. Currently, clearing methods that can be applied to live/ intact samples are being investigated in other fields, and it will be interesting to optimize optical mosquito clearance accordingly. The results presented here will hopefully fuel the development of whole-body imaging technologies to allow for the discovery of important host-pathogen interactions in the malaria field and beyond.

Author contributions

MDN and JK performed mosquito infections and mosquito clearance. MDN and FM imaged mosquitoes by OPT. MDN, JK and EGS imaged mosquitoes by LSFM. MDN and JK reconstructed images. NMB generated diagrams. EGS, JVS and FF coordinated experiments. MDN and FF wrote the manuscript with input by all coauthors.

Acknowledgements

We are grateful to Prof. Volker Heussler (IZB, University of Bern) for his intellectual input and funding of this project. We thank Dr. Renzo Danuser (Theodor Kocher Institute, University of Bern) for important input for the OPT technique, and Dr. Leandro Lemgruber (Wellcome Trust Centre for Molecular Parasitology) for his input on image processing. OPT and confocal microscopy was performed on equipment supported by the Microscopy Imaging Center, University of Bern, Switzerland. We thank Ernst Stelzer and Pavel Tomancak for motivation to use SPIM. This work was supported by the European Union's Seventh Framework Programme (FP7/2007-2013) under grant agreement 242095: EVIMalar (Prof. Volker Heussler and MDN), by a Swiss National Foundation Grant (310030_159519 to Prof. Volker Heussler) and an ERC starting grant (StG 281719) and the Chica and Heinz Schaller Foundation (FF).

Bibliography

Abe, J., Ozga, A.J., Swoger, J., Sharpe, J., Ripoll, J., Stein, J. V, 2016. Light sheet fluorescence microscopy for in situ cell interaction analysis in mouse lymph nodes. *J. Immunol*. Methods 431, 1–10. doi:http://dx.doi.org/10.1016/j.jim.2016.01.015

Aly, A.S.I., Vaughan, A.M., Kappe, S.H.I., 2009. Malaria parasite development in the mosquito and infection of the mammalian host. *Annu. Rev. Microbiol*. 63, 195–221. doi:10.1146/annurev.micro.091208.073403

Baldini, F., Gabrieli, P., South, A., Valim, C., Mancini, F., Catteruccia, F., 2013. The interaction between a sexually transferred steroid hormone and a female protein regulates oogenesis in the malaria mosquito Anopheles gambiae. *PLoS Biol* 11, e1001695. doi:10.1371/journal.pbio.1001695

Beaty, B.J., Marquardt, W.C., 1996. The biology of disease vectors. University Press of Colorado, Niwot, CO.

Becker, K., Jährling, N., Saghafi, S., Weiler, R., Dodt, H.-U., 2012. Chemical Clearing and Dehydration of GFP Expressing Mouse Brains. *PLoS One* 7(3): e33916. doi: 10.1371/journal.pone.0033916

Burda, P.-C., Roelli, M.A., Schaffner, M., Khan, S.M., Janse, C.J., Heussler, V.T., 2015. A Plasmodium phospholipase is involved in disruption of the liver stage parasitophorous vacuole membrane. *PLoS Pathog* 11(3): e1004760. doi: 10.1371/journal.ppat.1004760

CDC, 2014. CDC Division of Vector-Borne Diseases [WWW Document]. URL http://www.cdc.gov/ncezid/dvbd/about.html (accessed 10.3.16).

Choumet, V., Carmi-Leroy, A., Laurent, C., Lenormand, P., Rousselle, J.-C., Namane, A., Roth, C., Brey, P.T., 2007. The salivary glands and saliva of Anopheles gambiae as an essential step in the Plasmodium life cycle: A global proteomic study. Proteomics 7(18): 3384–3394. doi:10.1002/pmic.200700334

Chung, K., Wallace, J., Kim, S.-Y., Kalyanasundaram, S., Andalman, A.S., Davidson, T.J., Mirzabekov, J.J., Zalocusky, K.A., Mattis, J., Denisin, A.K., Pak, S., Bernstein, H., Ramakrishnan, C., Grosenick, L., Gradinaru, V., Deisseroth, K., 2013. Structural and molecular interrogation of intact biological systems. Nature 497 (7449): 332–337. doi: 10.1038/nature12107

De Niz, M., Spadin, F., Marti, M., Stein, J. V, Frenz, M., Frischknecht, F., 2019. Toolbox for in vivo imaging of host–parasite interactions at multiple scales. *Trends Parasito*l. 35 (3): 193–212. doi:https://doi.org/10.1016/j.pt.2019.01.002

Dodt, H.-U., Leischner, U., Schierloh, A., Jahrling, N., Mauch, C.P., Deininger, K., Deussing, J.M., Eder, M., Zieglgansberger, W., Becker, K., 2007. Ultramicroscopy: three-dimensional visualization of neuronal networks in the whole mouse brain. *Nat Meth* 4(4): 331–336. doi: 10.1038/nmeth1036.

Eldridge, B.F., Edman, J.D., 2000. Medical Entomology. Dordrecht, The Netherlands: Kulwer Academic Publishers.

Ertürk, A., Becker, K., Jährling, N., Mauch, C.P., Hojer, C.D., Egen, J.G., Hellal, F., Bradke, F., Sheng, M., Dodt, H.-U., 2012. Three-dimensional imaging of solvent-cleared organs using 3DISCO. *Nat. Protoc.* 7(11): 1983–1995. doi: 10.1038/nprot.2012.119.

Frischknecht, F., Martin, B., Thiery, I., Bourgouin, C., Menard, R., 2006. Using green fluorescent malaria parasites to screen for permissive vector mosquitoes. *Malar. J.* 5:23, 1–8. doi:10.1186/1475-2875-5-23

Frischknecht, F., Mota, M., Scherf, A., Waters, A., 2014. Biology of the Malaria Parasite – editorial on the special issue for the 10th BioMalPar conference. *Cell. Microbiol.* 16(5), 599–601. doi:10.1111/cmi.12295

Genina, E.A., Bashkatov, A.N., Tuchin, V. V, 2010. Tissue optical immersion clearing.

Expert Rev. Med. Devices 7, 825–842. doi:10.1586/erd.10.50
Gerger, A., Koller, S., Kern, T., Massone, C., Steiger, K., Richtig, E., Kerl, H., Smolle, J., 2005. Diagnostic Applicability of In Vivo Confocal Laser Scanning Microscopy in Melanocytic Skin Tumors. *J. Invest. Dermatol.* 124 (3): 493–498. doi:http://dx.doi.org/10.1111/j.0022-202X.2004.23569.x
Gualda, E.J., Vale, T., Almada, P., Feijó, J.A., Martins, G.G., Moreno, N., 2013. OpenSpinMicroscopy: an open-source integrated microscopy platform. *Nat. Methods* 10 (7): 599-600. doi: 10.1038/nmeth.2508.
Ha, Y.-R., Lee, S.-C., Seo, S.-J., Ryu, J., Lee, D.-K., Lee, S.-J., 2015. Comparison of the functional features of the pump organs of Anopheles sinensis and Aedes togoi. *Sci. Rep.* 5, 15148. doi: 10.1038/srep15148.
Hama, H., Hioki, H., Namiki, K., Hoshida, T., Kurokawa, H., Ishidate, F., Kaneko, T., Akagi, T., Saito, T., Saido, T., Miyawaki, A., 2015. ScaleS: an optical clearing palette for biological imaging. *Nat Neurosci* 18(10): 1518–1529. doi: 10.1038/nn.4107.
Hama, H., Kurokawa, H., Kawano, H., Ando, R., Shimogori, T., Noda, H., Fukami, K., Sakaue-Sawano, A., Miyawaki, A., 2011. Scale: a chemical approach for fluorescence imaging and reconstruction of transparent mouse brain. *Nat Neurosci*. 14 (11), 1481–1488. doi: 10.1038/nn.2928.
Huisken, J., Swoger, J., Del Bene, F., Wittbrodt, J., Stelzer, E.H.K., 2004. Optical sectioning deep inside live embryos by selective plane illumination microscopy. *Science.* 305(5686), 1007–1009. doi:10.1126/science.1100035
Jährling, N., Becker, K., Schönbauer, C., Schnorrer, F., Dodt, H.-U., 2010. Three-dimensional reconstruction and segmentation of intact Drosophila by ultramicroscopy. *Front. Syst. Neurosci.* 4: 1. doi:10.3389/neuro.06.001.2010
Kak, A.C., Slaney, M., 1988. Principles of Computerized Tomographic Imaging. IEEE Press.
Ke, M.-T., Fujimoto, S., Imai, T., 2013. SeeDB: a simple and morphology-preserving optical clearing agent for neuronal circuit reconstruction. *Nat Neurosci* 16 (8): 1154–1161. doi:10.1038/nn.3447.
Kettle, D.S., 1995. Medical and veterinary entomology. University Press, Cambridge.
Krenn, H.W., Aspöck, H., 2012. Form, function and evolution of the mouthparts of blood-feeding Arthropoda. Arthropod Struct. Dev. 41(2): 101–118. doi:http://dx.doi.org/10.1016/j.asd.2011.12.001
Lefevre, T., Thomas, F., Schwartz, A., Levashina, E., Blandin, S., Brizard, J.-P., Le Bourligu, L., Demettre, E., Renaud, F., Biron, D.G., 2007. Malaria Plasmodium agent induces alteration in the head proteome of their Anopheles mosquito host. Proteomics 7(11): 1908–1915. doi:10.1002/pmic.200601021
Lehane, M.J., 1991. Biology of Blood-sucking insects. Harper Collins Academic.
Macdonald, G., 1956. Theory of the eradication of malaria. Bull. World Health Organ. 15, 369–387.
Maekawa, E., Aonuma, H., Nelson, B., Yoshimura, A., Tokunaga, F., Fukumoto, S., Kanuka, H., 2011. The role of proboscis of the malaria vector mosquito Anopheles stephensi in host-seeking behavior. *Parasit Vectors* 4, 10. doi:10.1186/1756-3305-4-10
Mayer, J., Robert-Moreno, A., Danuser, R., Stein, J.V., Sharpe J., Swoger, J., 2014. OPTiSPIM: integrating optical projection tomography in light sheet microscopy extends specimen characterization to nonfluorescent contrasts. *Opt. Lett.* 39 (4): 1053–1056. doi: 10.1364/OL.39.001053.
McGurk, L., Morrison, H., Keegan, L.P., Sharpe, J., O'Connell, M.A., 2007. Three-Dimensional Imaging of Drosophila melanogaster. *PLoS One* 2, e834. doi:10.1371/journal.pone.0000834
Mitchell, S.N., Kakani, E.G., South, A., Howell, P.I., Waterhouse, R.M., Catteruccia, F.,

2015. Evolution of sexual traits influencing vectorial capacity in anopheline mosquitoes. *Science* 347 (6225): 985–988. doi:10.1126/science.1259435

Mori, T., Hirai, M., Mita, T., 2019. See-through observation of malaria parasite behaviors in the mosquito vector. *Sci. Rep.* 9, 1768. doi:10.1038/s41598-019-38529-3

Ntziachristos, V., 2010. Going deeper than microscopy: the optical imaging frontier in biology. *Nat Meth* 7, 603–614. doi:10.1038/nmeth.1483.

Pampaloni, F., Reynaud, E.G., Stelzer, E.H.K., 2007. The third dimension bridges the gap between cell culture and live tissue. *Nat Rev Mol Cell Biol* 8 (10): 839–845. doi:10.1038/nrm2236.

Pitrone, P.G., Schindelin, J., Stuyvenberg, L., Preibisch, S., Weber, M., Eliceiri, K.W., Huisken, J., Tomancak, P., 2013. OpenSPIM: an open-access light-sheet microscopy platform. *Nat Meth* 10 (7): 598–599. doi:10.1038/nmeth.2507.

Poguzhelskaya, E., Artamonov, D., Bolshakova, A., Vlasova, O., Bezprozvanny, I., 2014. Simplified method to perform CLARITY imaging. *Mol. Neurodegener.* 9, 19. doi:10.1186/1750-1326-9-19

Prado, M., Eickel, N., De Niz, M., Heitmann, A., Agop-Nersesian, C., Wacker, R., Schmuckli-Maurer, J., Caldelari, R., Janse, C.J., Khan, S.M., May, J., Meyer, C.G., Heussler, V.T., 2015. Long-term live imaging reveals cytosolic immune responses of host hepatocytes against Plasmodium infection and parasite escape mechanisms. *Autophagy* 11 (9): 1561–1579. doi:10.1080/15548627.2015.1067361

Ribeiro, J.M., Rossignol, P.A., Spielman, A., 1984. Role of mosquito saliva in blood vessel location. *J. Exp. Biol.* 108, 1-7.

Rono, M.K., Whitten, M.M.A., Oulad-Abdelghani, M., Levashina, E.A., Marois, E., 2010. The major yolk protein vitellogenin interferes with the anti-Plasmodium response in the malaria mosquito Anopheles gambiae. *PLoS Biol* 8 (7): e1000434. doi: 10.1371/journal.pbio.1000434.

Rossignol, P.A., Ribeiro, J.M.C., Spielman, A., 1984. Increased Intradermal Probing Time in Sporozoite-Infected Mosquitoes. *Am. J. Trop. Med. Hyg.* 33 (1): 17–20. doi:10.4269/ajtmh.1984.33.17.

Sharpe, J., Ahlgren, U., Perry, P., Hill, B., Ross, A., Hecksher-Sørensen, J., Baldock, R., Davidson, D., 2002. Optical Projection Tomography as a Tool for 3D Microscopy and Gene Expression Studies. *Science.* 296 (5567): 541-545. doi:10.1126/science.1068206.

Silvie, O., Mota, M.M., Matuschewski, K., Prudêncio, M., 2008. Interactions of the malaria parasite and its mammalian host. *Curr. Opin. Microbiol.* 11 (4): 352–359. doi:http://dx.doi.org/10.1016/j.mib.2008.06.005

Smith, D.L., Battle, K.E., Hay, S.I., Barker, C.M., Scott, T.W., McKenzie, F.E., 2012. Ross, Macdonald, and a Theory for the Dynamics and Control of Mosquito-Transmitted Pathogens. *PLoS Pathog* 8 (4): 1–13. doi:10.1371/journal.ppat.1002588

Susaki, E.A., Tainaka, K., Perrin, D., Kishino, F., Tawara, T., Watanabe, T.M., Yokoyama, C., Onoe, H., Eguchi, M., Yamaguchi, S., Abe, T., Kiyonari, H., Shimizu, Y., Miyawaki, A., Yokota, H., Ueda, H.R., 2016. Whole-brain imaging with single-cell resolution using chemical cocktails and computational analysis. *Cell,* 157 (3): 726–739. doi:10.1016/j.cell.2014.03.042

Takken, W., Knols, B.G.J., 1999. Odor-mediated behavior of Afrotropical malaria mosquitoes. *Annu. Rev. Entomol.* 44, 131–157. doi:10.1146/annurev.ento.44.1.131

Vallejo Ramirez, P.P., Zammit, J., Vanderpoorten, O., Riche, F., Blé, F.-X., Zhou, X.-H., Spiridon, B., Valentine, C., Spasov, S.P., Oluwasanya, P.W., Goodfellow, G., Fantham, M.J., Siddiqui, O., Alimagham, F., Robbins, M., Stretton, A., Simatos, D., Hadeler, O., Rees, E.J., Ströhl, F., Laine, R.F., Kaminski, C.F., 2019. OptiJ: Open-source optical projection tomography of large organ samples. *bioRxiv* 656488. doi:10.1101/656488

Whitten, M.M.A., Shiao, S.H., Levashina, E.A., 2006. Mosquito midguts and malaria: cell biology, compartmentalization and immunology. Parasite Immunol. 28 (4), 121–130. doi:10.1111/j.1365-3024.2006.00804.x

WHO, 2015. World Malaria Report.

Won Jung, J., Baeck, S.-J., Perumalsamy, H., Hansson, B.S., Ahn, Y.-J., Kwon, H.W., 2015. A novel olfactory pathway is essential for fast and efficient blood-feeding in mosquitoes. *Sci. Rep.* 5, 13444. doi: 10.1038/srep13444.

Figure 1

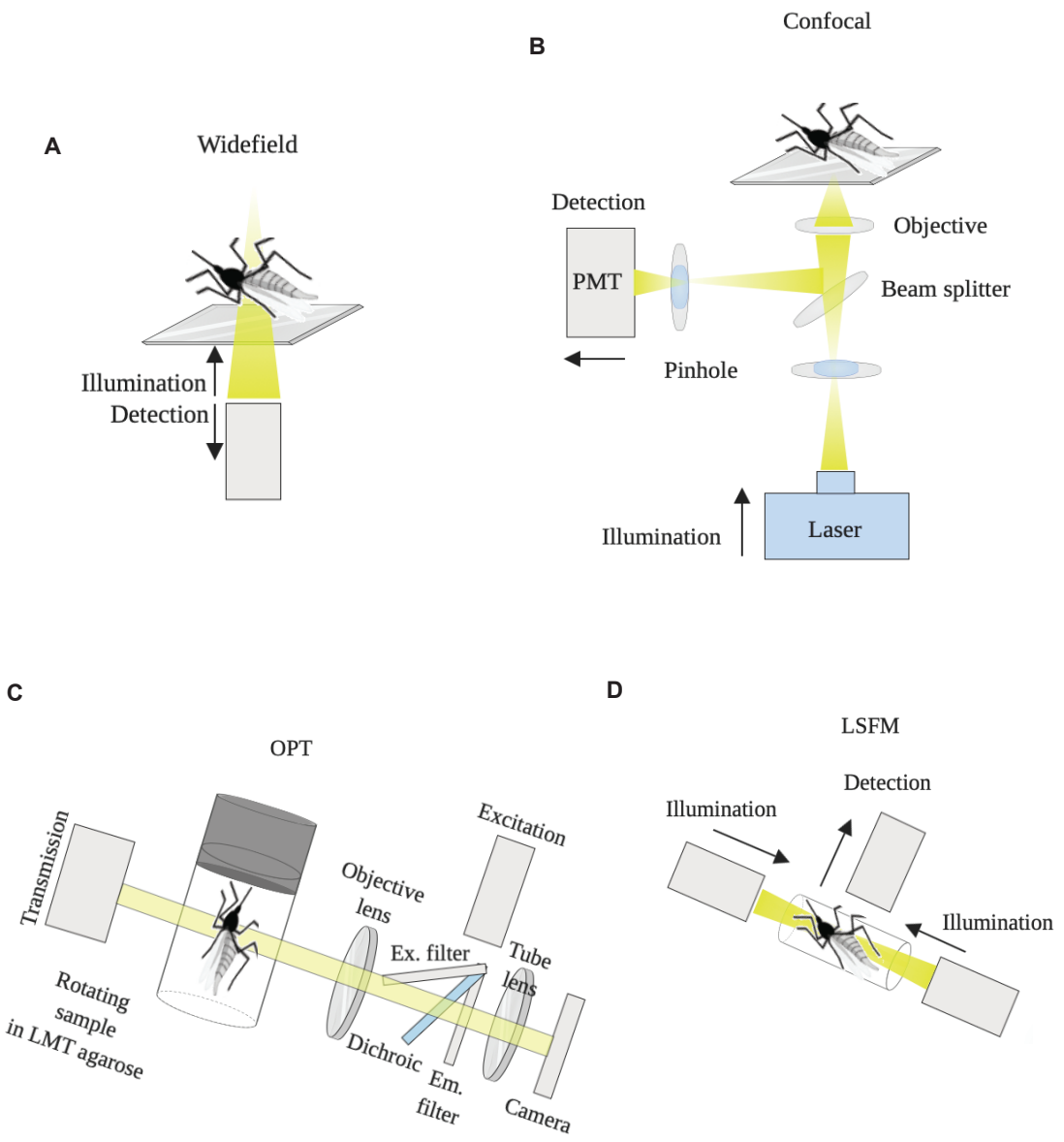

Figure 1. Microscopy methods used for imaging mosquitoes. **(A)** Principle of widefield microscopy. The entire specimen is exposed to the light source, and is illuminated either from above (inverted microscope) or below (upright microscope). Widefield microscopes are composed of a white and fluorescence light source, a microscope and a camera. **(B)** Principle of confocal microscopy. The light source for excitation comes from laser units. The confocal system contains pinholes to exclude out of focus light, dichroic mirrors to filter light of certain wavelengths (while reflecting others), and photomultiplier tubes (PMTs), to collect photons. **(C)** Principle of OPT. The optically cleared specimen

is embedded in agarose, attached to a metallic cylinder within a rotating stage, and suspended in an index-matching liquid to reduce scattering and heterogeneities of refractive index throughout the specimen. When the specimen is rotated to a series of angular positions, images are captured at each orientation. The setup is aligned to ensure that the axis of rotation is perpendicular to the optical axis, so that straight line projections going through the sample can be generated, and collected by pixels on the CCD of the camera. **(D)** Principle of LSFM. The optically cleared sample is embedded in agarose, and suspended within a sample holder inside an index-matching liquid. A thin (μm range) slice of the sample is illuminated perpendicularly to the direction of observation. Scanning is performed using a plane of light, which allows very fast image acquisition.

Figure 2

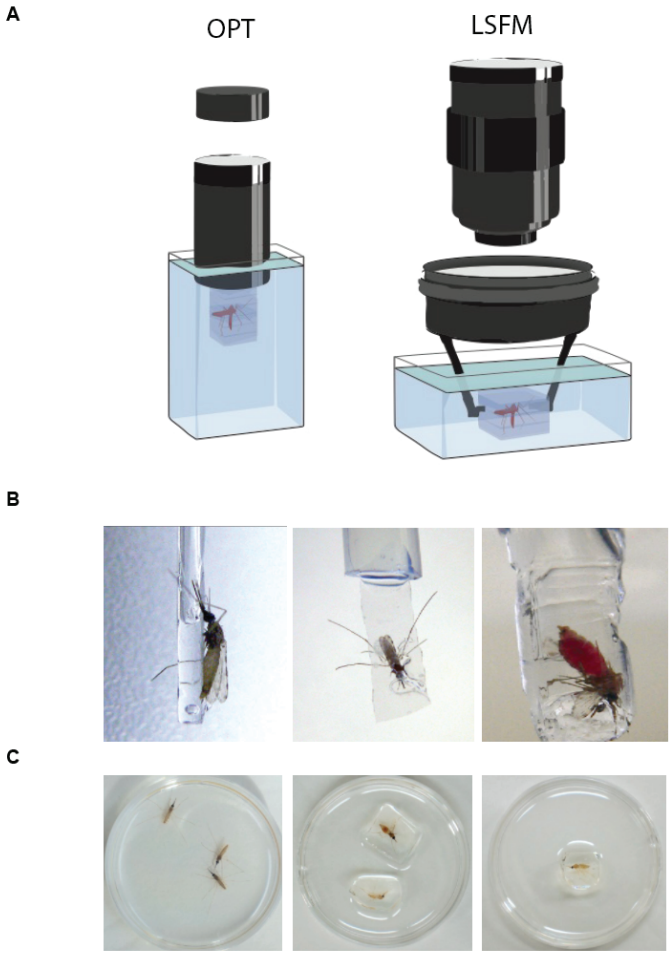

Figure 2. Mosquito mounting and embedding. **(A)** OPT imaging requires embedding the mosquito in low-melting temperature ultrapure agarose gel, and mounting it onto a metallic cylinder that is attached to a rotating stage via a magnet. The embedded attached mosquito is then lowered into a chamber containing index-matching liquid, such as Murray's clear medium. The setup for Ultramicroscopy imaging involves embedding the mosquito in low-melting temperature ultrapure agarose gel, and mounting it on a lower ring of the customized holder. Both the holder and the embedded mosquito are submerged into a chamber containing index-matching liquid. **(B)** Methods for mounting mosquitoes to enable imaging and rotation. **(C)** Petri dishes showing (1) fixed mosquitoes prior to optical clearance and embedding and (2) optically cleared mosquitoes embedded in ultrapure low-melting temperature agarose.

Figure 3

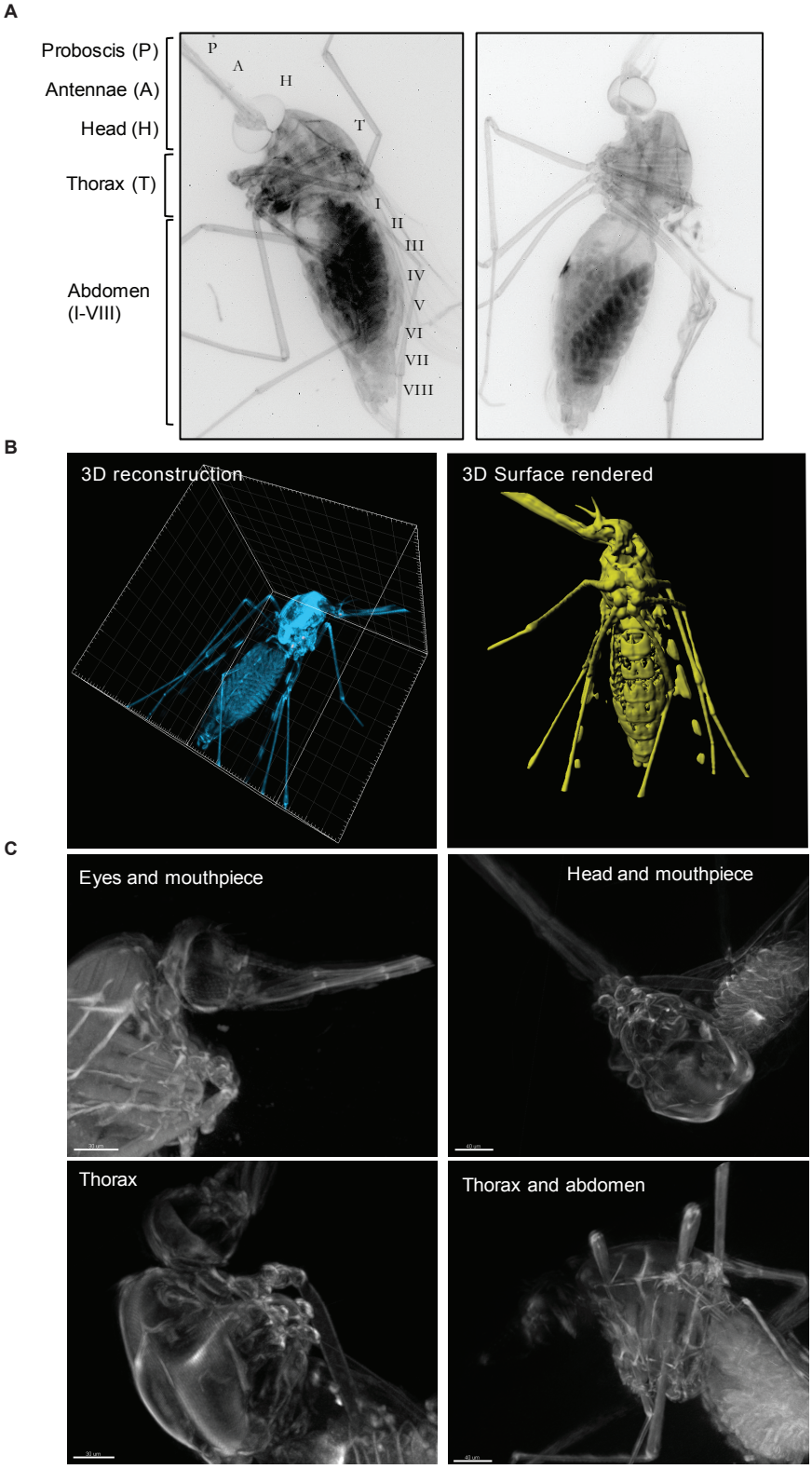
A
Proboscis (P)
Antennae (A)
Head (H)
Thorax (T)
Abdomen
(I-VIII)
P
A
H
T
I
II
III
IV
V
VI
VII
VIII
B
3D reconstruction
3D Surface rendered
C
Eyes and mouthpiece
Head and mouthpiece
Thorax
Thorax and abdomen

Figure 3. Visualization of an optically cleared *Anopheles stephensi* female mosquito. **(A)** 2D reconstruction of two reconstructed mosquitoes showing detailed views of the head structures (H) including the antennae (A), and the proboscis (P) and the eyes. Detailed view of the thorax is also possible, as well as of all segments of the abdomen. **(B)** 3D reconstruction and clear view of all body cavities of an optically cleared mosquito (left panel). 3D reconstruction and rendering of the mosquito (right panel) clearly showing abdominal segments, thorax and head features (previously shown in (De Niz et al., 2019)). **(C)** Close-up views of various views of the optically cleared mosquito body including the eyes and mouthpieces (side view, upper left panel), the head and mouthpiece (top view, upper right panel), the thorax (side view, lower left panel), and the abdomen including eggs (side view, lower right panel).

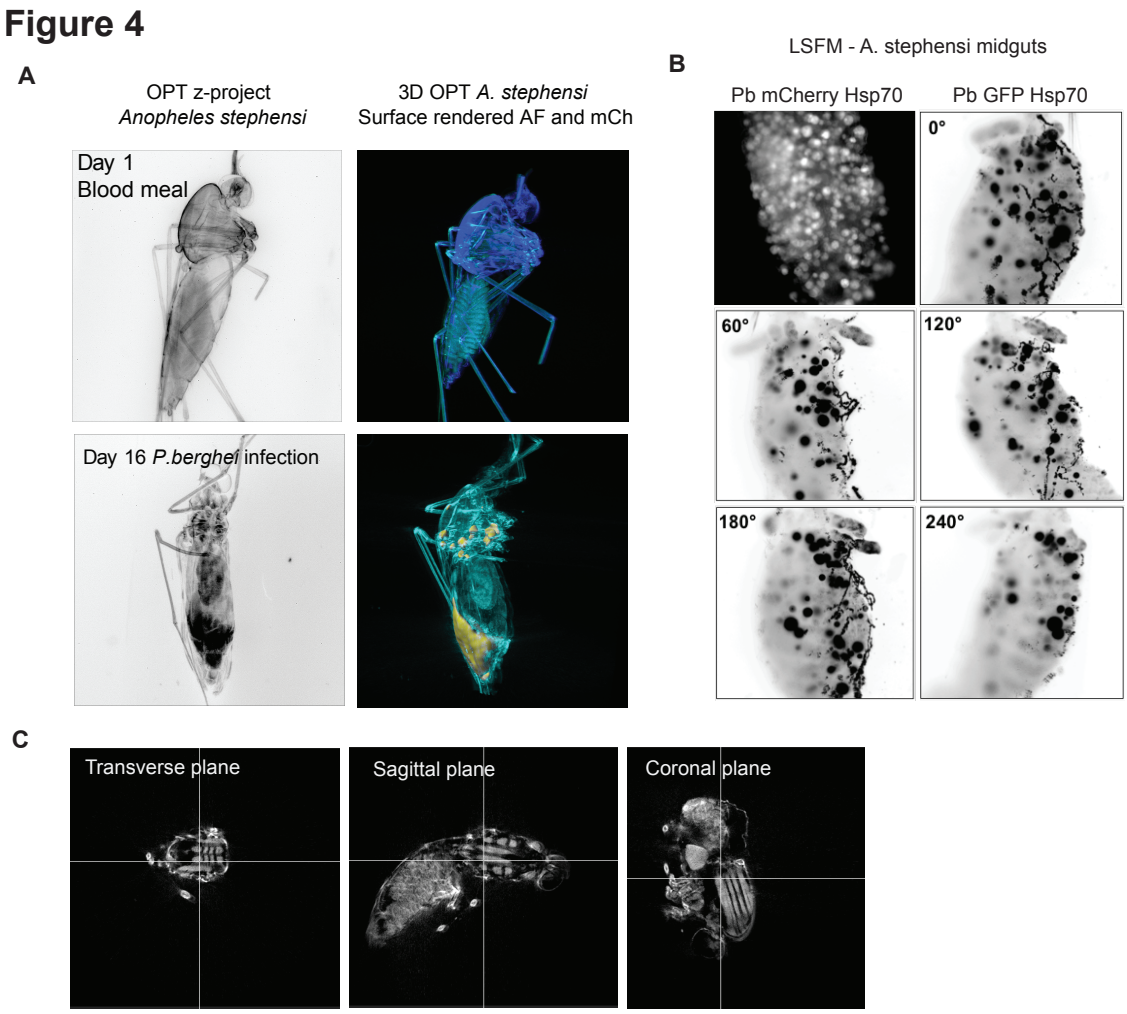

Figure 4. Visualization of *Plasmodium*-infected *Anopheles stephensi* female mosquitoes. **(A)** 3D project (B&W) and 3D reconstructions of mosquitoes at the beginning and end of *P. berghei* infection as well as egg development. **(B)** *P. berghei*-infected mosquito midguts imaged by LSFM. Oocysts are shown in white (*P. berghei*-mCherry) or black (*P. berghei*-GFP). **(C)** Sagittal, coronal and transverse sections of a single position in the entire, optically cleared mosquito.

Movie 1. 3D visualization of an optically cleared *Anopheles stephensi* female mosquito, imaged by optical projection tomography.